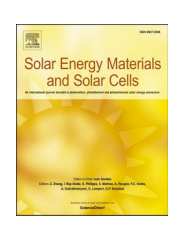
ELSEVIER

Contents lists available at ScienceDirect

Solar Energy Materials and Solar Cells

journal homepage: www.elsevier.com/locate/solmat





Transparent porphyrin-based hybrid films for spectral selective solar harvesting and energy generation

Jou Lin, Yuxin Wang, Mengyao Lyu, Zicheng Deng, Donglu Shi

The Materials Science and Engineering Program, Department of Mechanical and Materials Engineering, College of Engineering and Applied Science, University of Cincinnati, Cincinnati, OH, 45221, USA

ABSTRACT

Spectral-selectively solar harvest is achieved in designated frequency regions for photothermal energy generation. In this study, we have designed and synthesized porphyrin-based hybrids that typically exhibit two absorption peaks respectively near 400 nm (blue-violet) and 700 nm (NIR). To be able to tune the optical absorptions for more efficient solar harvest especially in the IR region, unique porphyrin hybrids are developed by incorporating another porphyrin compound such as phthalocyanine, and inorganic Fe_3O_4 @Cu_{2-x}S nanoparticles with different absorption characteristics. By controlling the ratio of the components, the hybrids exhibit gradual and consistent changes in the optical spectra, showing high spectral tunability. Transparent thin films of the hybrids are deposited on glass substrates and assembled in parallel for 3D solar harvesting in a cuboid photothermal generator. Solar light is able to pass through the multilayers of thin films, generating significant thermal heat on each one for enhanced energy density. The structural features of the hybrids are well correlated to the optical behaviors based on Raman studies. Also discussed is the operating mechanisms underlying the photothermal behaviors associated with the hybrid structures.

1. Introduction

To meet the mission of net-zero by 2050, declared at COP26, creating an energy neutral, zero emission, and climate positive civic infrastructure has become the highest priority in clean and renewable energy research. Solar light can be converted to various energy forms including heat, electricity, and biochemical energies for a wide range of applications [1]. The solar spectra are widely divided into three regions: ultraviolet (UV), visible, and infrared (IR), with corresponding wavelengths: 100-400 nm, 400-700 nm, and above 700 nm. About 58% of the energy density of the solar spectrum lies below 800 nm with the other 42% occurring at longer wavelengths [1-4]. As is well-known, photovoltaic (PV) mainly utilizes the UV and visible (UV/Vis), while the IR part is majorly converted to heat [2]. This absorbed long-wavelength solar energy contributes to heating of the PV which causes considerable efficiency decreases [3-8]. However, the IR portion of the solar light can be utilized to generate heat for thermoelectric and photothermal energy applications.

The current PV technologies have achieved efficiencies on the order of 25% [9–14]. There are other possible alternative ways of utilizing solar energy such as the spectral selective photothermal energy generation [15]. One of the photothermal energy applications is the so-called Optical Thermal Insulation (OTI) based on a transparent photothermal coating on single pane widow without any intervention media. Two

types of photothermal thin films, namely iron oxides and porphyrin compounds, can selectively harvest solar light in the UV and NIR regions, while maintaining 85% average visible transmittance (AVT). The photothermal coating can generate sufficient heat on window surfaces, thus lowering the temperature difference between the single-pane and room interior, and significantly reduce thermal transmittance. With OTI, single-pane window is highly possible in cold climate without any glazing technologies and intervention media [16].

Photothermal (PT) materials have been mainly applied in medical therapeutics such as photothermal therapy (PTT) [17–20]. With a small quantity of nanoparticles up taken by the tumor, upon near-infrared (NIR) laser excitation, the local temperature in the lesions can reach $\sim45\,^{\circ}\mathrm{C}$ which can kill the cancer cells effectively. In energy applications such as OTI, the PT materials are utilized to absorb solar light in the UV and NIR regions for both high photothermal efficiency and visible transparency [15,21–26]. The PT materials include inorganic materials (i.e. noble metals [27,28], carbon-based materials [29,30], metal oxide and its composites [15,21,24–26], and organic materials (i.e. polymer-based nanomaterials) [31].

Upon solar harvesting, the photothermal materials can be photonically-activated to generate thermal energy directly and efficiently for many energy applications such as energy-efficient building skins [23–25], photothermal energy generator [26], and photothermal desalination [32,33]. However, most of the current photothermal

E-mail address: shid@ucmail.uc.edu (D. Shi).

^{*} Corresponding author.

materials are based on metallic compounds and graphene that are either dark or non-transparent, therefore limiting solar harvesting to 2D surfaces. A fundamental question to be asked is whether sunlight can be collected through multiple layers if they are rendered transparent. This possibility lies on the spectral selective and tunable nanostructures that not only exhibit strong UV and NIR absorptions, but also high average visible transmittance (AVT). With these unique optical characteristics, it is highly possible that solar harvesting will profoundly transform from 2D to 3D with much greater energy density. Currently, several transparent photothermal thin films have been developed for multilayer solar harvesting and energy generation, resulting in significant increase in photon collecting surface areas and energy density [26]. This novel method will fundamentally lift the current limitations in 2D surface solar harvesting by introducing another dimensionality via transparent thin films. The thermal energy generated in a confined volume can be further utilized to produce electricity, or other forms of energy for a variety of applications, including utility heating and thermoelectric devices. Spectrally selective photothermal thin films allow more efficient utilization of solar light; while the UV/vis portions for PV, the IR can be used for thermal energy applications. This will pave a new path to spectral selective solar harvesting and energy generation.

Recently, a class of porphyrin compounds has been found to exhibit strong photothermal effects under both NIR laser and white light irradiation [23-25]. They have been applied in PV applications for their appreciable photon conversion efficiency (PCE) due to the donor-acceptor framework [34,35]. Porphyrins contain a large ring molecule constituted of tetrapyrrole, which is made from four carbons and one nitrogen, and with a metal ion at the center of the tetrapyrrole ring. Due to unique chemical structures of the porphyrin compounds, they typically exhibit two main peaks in the absorption spectra, which are the B band (380-500 nm) and the Q band (500-750 nm). Chlorophyll is an essential component in the plants for photosynthesis, which is characterized with a unique "saddle-like" absorption spectrum with a higher absorption peak at 413 nm and a lower one at 668 nm. Chlorophyllin is derived from chlorophyll with the center atom of divalent copper instead of magnesium. As a derivative of chlorophyll, chlorophyllin shows similar absorption peaks to those of chlorophyll at 402 nm and 628 nm. Replacing the center atom with copper results in phthalocyanine with considerably modified absorption peaks at 350 nm, 638 nm, and 730 nm [23]. The photothermal mechanism of porphyrins has been identified to be associated with the photon-activated vibrations of the porphyrin molecules [23]. These transparent PT films can be developed for spectral-selective solar harvest and energy generation.

In this study, novel hybrids were designed and developed between two fundamentally different families of materials, namely porphyrins and iron oxides in order to manipulate their spectra in a wide range. The structural features were investigated by Raman spectroscopy through consistent compositional variations of the components. The optical absorptions of the hybrids were structurally tuned via compositional combinations between different porphyrins and oxides. A photothermal generator (PTG) was designed and engineered to spectral-selectively harvest solar light in a 3D space. The PTG photothermal parameters of hybrids were calculated including the total energy generated, the power of the PTG, and energy density.

2. Experimental procedures

Material Synthesis: Chlorophyllin sodium copper was purchased from Sigma-Aldrich and β-form copper phthalocyanine was purchased from Tokyo Chemical Industry Co., Ltd. Iron (III) acetylacetonate (Fe(acac)₃, \geq 99.9%), copper (II) acetylacetonate (Cu (acac)₂, \geq 99.9%), oleylamine (70%), sulfur (99.998%), N-methyl-2-pyrrolidone (99.5%), chloroform (\geq 99.9%), tetrahydrofuran (THF, \geq 99.9%), and polyethylene glycol (PEG, Mw = 6000) were purchased from Sigma-Aldrich Inc. (Milwaukee, WI, USA). Cyclohexane was purchased from Tedia Inc. (Fairfield, OH, USA).

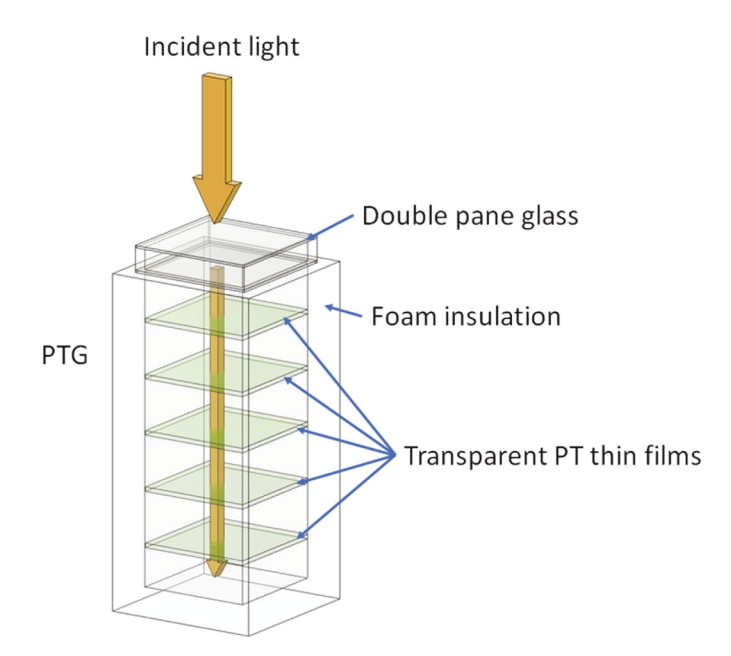


Fig. 1. Schematic digram showing the multilayer photothermal thin film structures of the photothermal-generator (PTG) for 3D solar harvesting and energy generation.

Fe₃O₄@Cu_{2-x}S nanoparticles were synthesized based on a modified procedure from the literature [36,37]. Briefly, 60 mL of oleylamine was heated to 300 °C and stirring for 30 min in a three-neck flask in a nitrogen environment to remove residual water and oxygen. Subsequently, a mixture (Mixture A) containing 12 mL of oleylamine, 8 mL of N-methyl-2-pyrrolidone, and 700 mg of Fe(acac)₃ was injected into the flask. Keeping the solution at 300 $^{\circ}$ C and stirring for 10 min, the mixture was cooled down to 70 °C. Meanwhile, another mixture (Mixture B) of 128.28 mg of sulfur dissolved in 12 mL of oleylamine was mixed with 10 mL of cyclohexane and injected into Mixture A to form Mixture C. After stirring Mixture C at 70 °C for 10 min, a solution containing 523.52 mg of Cu(acac)₂, 4 mL of oleylamine, and 16 mL of chloroform solution was injected into it as the final mixture. The final mixture was kept at 70 $^{\circ}\text{C}$ and stirred for 30 min, and ready for transferring to a beaker. The Fe₃O₄@Cu_{2-x}S nanoparticles were collected by a strong magnet and washed three times with methanol, and then freeze-dried overnight. After drying, nanoparticles were dispersed in THF for later use. The glass substrates (2.54 \times 2.54 \times 0.1 cm³) were cleaned in acetone and isopropanol for 15 min by ultrasonic cleaner, and then dried by compressed air.

Thin Film Deposition: Solutions containing various chlorophyllin to phthalocyanine and chlorophyllin to Fe_3O_4 @ $Cu_{2.x}S$ ratios were incorporated into THF with 10 wt% PEG. Thin films were deposited onto glass substrates with the solutions of different hybrids by spin-coating at 3000 rpm for 10 s. The as-deposited films were uniform in thickness (\sim 500–800 nm) with high uniformity and transparency.

<u>Photothermal Experiments</u>: The thin film samples were irradiated by 0.1 W/cm² white light using the Newport 150 W solar simulator (Lamp model 67005). The light power density was measured by using an optical power meter (Newport, 1919-R). The thin film temperature was recorded by an infrared camera (FLIR E6). A black sheet was placed under the sample to avoid reflection of light. There are two main steps in this experiment, namely, heating and cooling. The shape and size of the light spot was set to exactly cover the sample surface.

Optical Property Characterization: The absorption and transmittance spectra were acquired by using a UV-VIS NIR spectrometer (Lambda 900, PerkinElmer Inc.). The average visible transmittance (AVT) was measured by a light transmittance meter LS116 (Linshang, Co. Ltd.).

Raman Spectroscopy: The Raman spectra were acquired by Raman

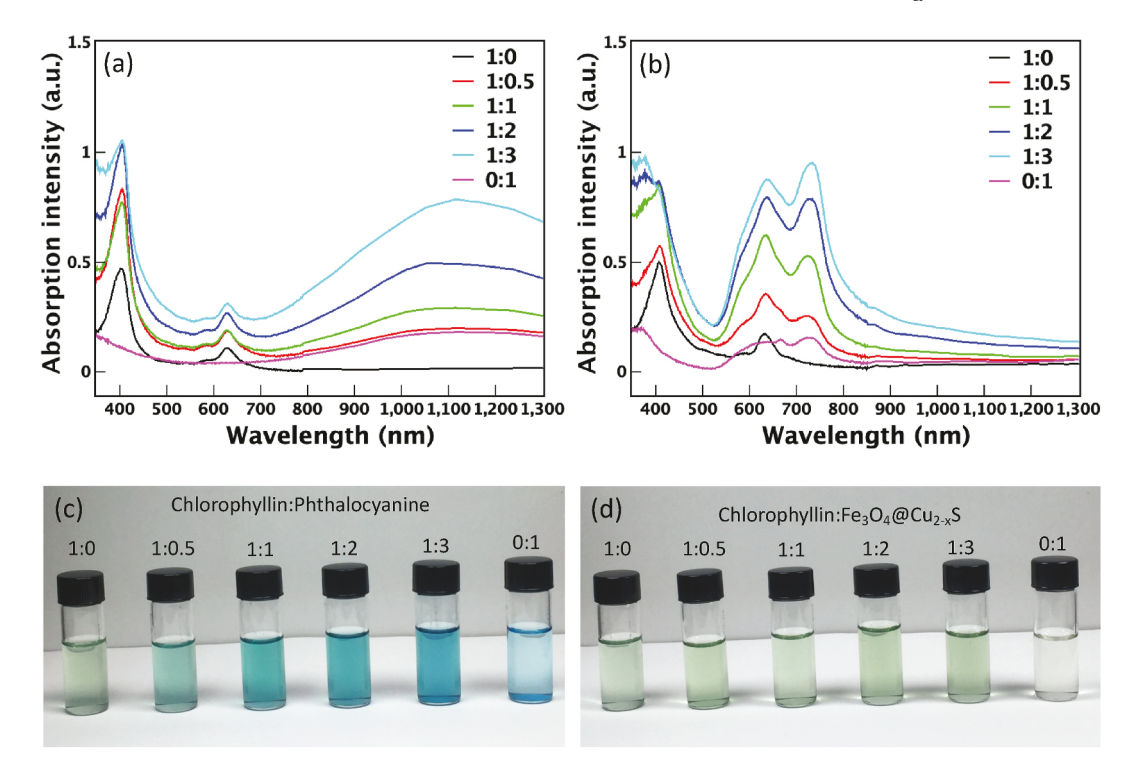


Fig. 2. Absorption spectra of the hybrid solutions of (a) Chlorophyllin:Phthalocyanine and (b) Chlorophyllin:Fe $_3$ O $_4$ @Cu $_2$. $_x$ S in THF. The base concentration of chlorophyllin is fixed at 0.01 mg/ml. The ratio formula on the top right corner represent the respective proportions of Chlorophyllin:Phthalocyanine (Fig. 2a) and Chlorophyllin:Fe $_3$ O $_4$ @Cu $_2$. $_x$ S (Fig. 2b). For instance, 1:0 denotes pure chlorophyllin and 0:1 denotes pure phthalocyanine in Fig. 2a; 1:0 denotes pure chlorophyllin and 0:1 denotes pure Fe $_3$ O $_4$ @Cu $_2$. $_x$ S in Fig. 2b. The concentrations of phthalocyanine and Fe $_3$ O $_4$ @Cu $_2$. $_x$ S are varied in the base solution of chlorophyllin, and denoted as 1:0.5, 1:1, 1:2, and 1:3. (c) Photographs of Chlorophyllin:Phthalocyanine in THF, and (d) photographs of Chlorophyllin:Fe $_3$ O $_4$ @Cu $_2$. $_x$ S in THF.

spectroscopy excited by 442 nm, 514 nm, and 633 nm lasers (Renishaw in Via). The sample holder for Raman spectroscopy was a microscope slide covered with an aluminum foil. The samples were drop-casted on aluminum foil twice to ensure the material was well-coated on the holder, and each drop was 2 μL .

<u>Photo-Thermal Generator Design and Assembly</u> A photo-thermal generator (PTG) was designed and assembled for the multilayer heating experiments. The transparent photothermal thin films were deposited on glass substrates of $25.4 \times 25.4 \times 1.4 \text{ mm}^3$. These PT-coated transparent substrates were positioned in parallel in a cuboid ($5 \times 5 \times 13 \text{ cm}^3$) which was thermally insolated (Fig. 1). The simulated solar light was directed from the top of the system, penetrating all the PT substrates, resulting in solar harvest in a three-dimensional fashion.

Since all layers were coated with the photothermal thin films, each generated thermal energy in the PTG.

3. Results

Since various porphyrin compounds exhibit quite different optical behaviors, their hybrids can provide wide ranges of spectra for controlled photonic behaviors via structural and compositional alterations. Quite successfully, hybrids of chlorophyllin:phthalocyanine and chlorophyllin:Fe₃O₄@Cu_{2-x}S were synthesized with gradual changes in optical absorptions. Fig. 2 shows the absorption spectra of the chlorophyllin:phthalocyanine and chlorophyllin:Fe₃O₄@Cu_{2-x}S hybrids with different proportions of phthalocyanine or Fe₃O₄@Cu_{2-x}S in THF. The

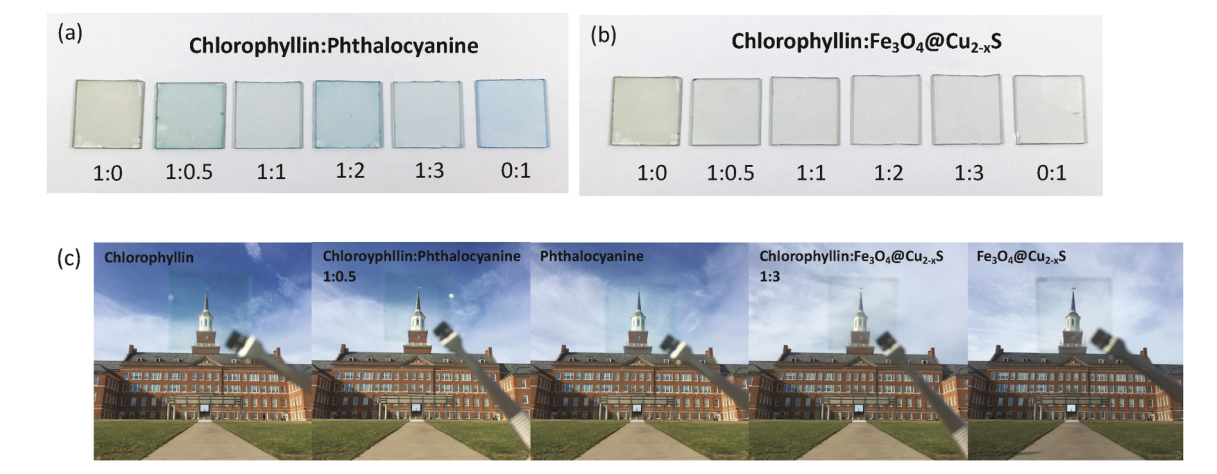


Fig. 3. Optical photographs of hybrid thin films of (a) Chlorophyllin:Phthalocyanine, (b) Chlorophyllin:Fe $_3$ O $_4$ @Cu $_2$ - $_x$ S deposited on glass substrate, and (c) in front of a campus building showing high transparencies of these films.

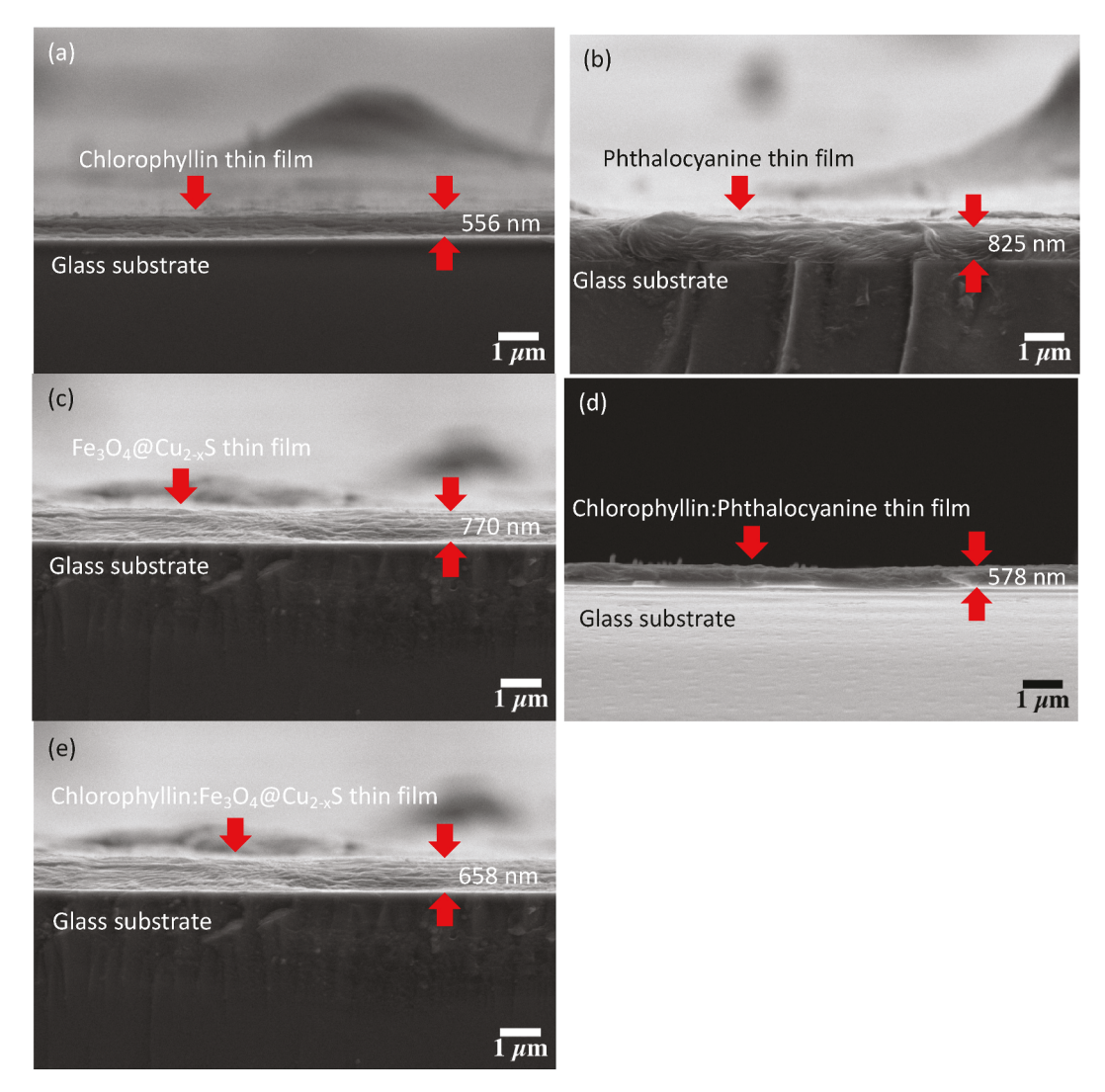


Fig. 4. Scanning electron microscopic (SEM) images of hybrid thin film cross-sectional areas of (a) chlorophyllin, (b) phthalocyanine, (c) $Fe_3O_4@Cu_{2-x}S$, (d) chlorophyllin:phthalocyanine, and (e) chlorophyllin: $Fe_3O_4@Cu_{2-x}S$.

concentration of chlorophyllin is fixed at 0.01 mg/mL and the amount of phthalocyanine or $Fe_3O_4@Cu_{2-x}S$ varies in the range of 0.000, 0.005, 0.010, 0.020, and 0.030 mg/mL, respectively. Note that 1:0 represents pure chlorophyllin, and 0:1 represents 100% phthalocyanine or 100% $Fe_3O_4@Cu_{2-x}S$ in THF. As shown in Fig. 2a, pure chlorophyllin (1:0, black curve) has an intensive absorption peak at 404 nm and a small one at 630 nm forming a so-called "saddle-like" spectrum. Phthalocyanine is however characterized with a moderate peak at 370 nm, and a broad absorption between 550 nm and 750 nm (0:1, pink curve). By increasing the proportion of phthalocyanine in the chlorophyllin solution, the peak of chlorophyllin at 404 nm is gradually shifted to 380 nm, while the 630 nm peak is not only broadened but also intensified with much stronger, and double-peaked absorption between 600 nm and 800 nm for the chlorophyllin:phthalocyanine ratio of 1:3 (cyan curve). The overall spectrum is significantly modified with a deep "U-shaped" valley.

 $Fe_3O_4@Cu_{2\cdot x}S$ is shown to have broad absorbance in both UV and NIR regions (1:0, pink curve in Fig. 1b). As shown in Fig. 2b, there is a wide absorption with a maximum at 1100 nm for $Fe_3O_4@Cu_{2\cdot x}S$ (0:1 pink curve), while no absorption in the IR region for chlorophyllin. By increasing the concentration of $Fe_3O_4@Cu_{2\cdot x}S$ in the chlorophyllin solution, the hybrids begin to develop more pronounced absorption peaks in both UV and IR regions. The hybrid with the 1:3 ratio exhibits strong and broad peaks at $\sim\!400$ nm and $\sim\!1100$ nm, which are much distinctive compared to their pure counterparts (i. e. 1:0 and 0:1). Interestingly, the

absorption peak of chlorophyllin at 630 nm is remained in the spectra of the chlorophyllin: Fe $_3$ O $_4$ @Cu $_2$. $_x$ S hybrids. Fig. 2c and d shows respectively the photographs of the chlorophyllin: phthalocyanine and chlorophyllin: Fe $_3$ O $_4$ @Cu $_2$. $_x$ S solutions with different ratios as indicated. As shown in these figures, both hybrid solutions are clear, transparent, and uniform without any aggregations or precipitates indicating homogeneous mixtures of the components. The data shown in Fig. 2 indicates the strong structural effects on optical spectral characteristics of the porphyrin compounds. By compositional alteration and optimization, the absorption of the hybrid can be well manipulated into desirable behaviors for specific solar-mediated energy applications.

Following the procedure described above, the hybrid solutions with various ratios of Chlorophyllin:Phthalocyanine and Chlorophyllin: Fe $_3O_4$ @Cu $_2$ - $_xS$ were deposited on glass substrates by spin coating. Fig. 3a and b shows the optical photographs of chlorophyllin, phthalocyanine, Fe $_3O_4$ @Cu $_2$ - $_xS$, and their hybrids in thin films. As can be seen, the colors of the thin films gradually change, corresponding to the different ratios of chlorophyllin:phthalocyanine and chlorophyllin: Fe $_3O_4$ @Cu $_2$ - $_xS$. These thin films are visually transparent in front of a campus building with AVT of 85% (Fig. 3c).

Fig. 4d–h shows the Scanning Electron Microscopy (SEM) images of the cross-sectional areas of the thin films, namely, chlorophyllin, phthalocyanine, Fe $_3$ O $_4$ @Cu $_2$. $_x$ S, chlorophyllin:phthalocyanine, and chlorophyllin:Fe $_3$ O $_4$ @Cu $_2$. $_x$ S. As shown in these SEM images, these films

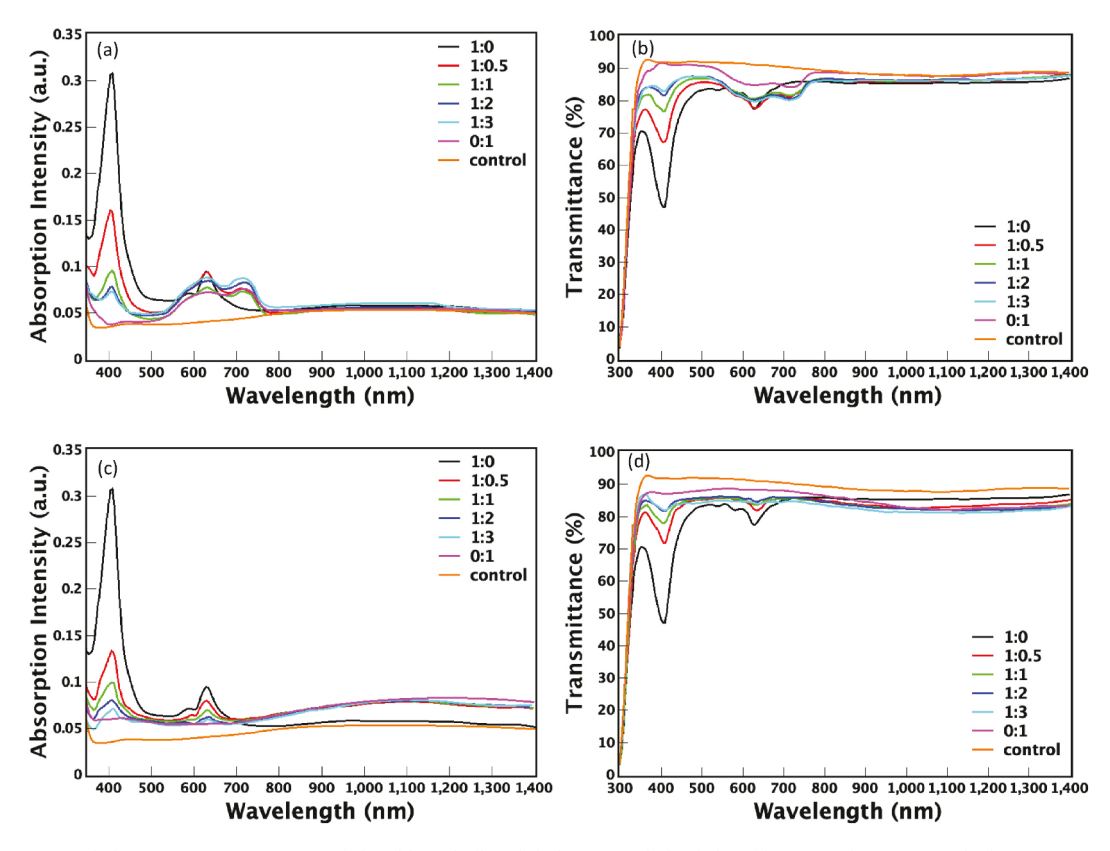


Fig. 5. (a) Absorption and (b) transmittance spectra of the chlorophyllin:phthalocyanine hybrid thin films; (c) Absorption and (d) transmittance spectra of the chlorophyllin: $Fe_3O_4@Cu_{2.x}S$ hybrid thin films.

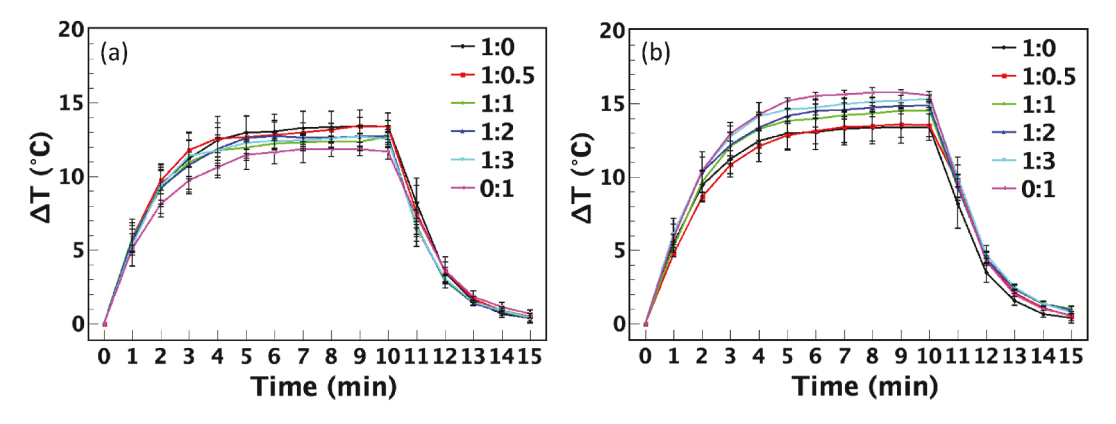


Fig. 6. Temperature vs. time curves of (a) Chlorophyllin:Phthalocyanine thin films and (b) Chlorophyllin:Fe $_3O_4$ @Cu $_2$ xS thin films with different ratios under white-light irradiation. AVTs of all films are kept at 85%. White light intensity is 0.1 W/cm². The room temperature is 22 °C.

are all uniform with smooth top surfaces and coherent interfaces with the substrates. The thicknesses of the films range between $\sim\!556$ nm and 825 nm, responsible for high transparency.

The as-deposited thin films were characterized by UV-vis/IR absorption and transmittance. Fig. 5 shows the UV-vis/IR transmittance and absorption spectra of the hybrid thin films. All thin film samples were controlled to exhibit AVT of 85%. A PEG coated thin film with 90% of AVT was used as control. As shown in Fig. 5, the absorption intensities of all thin films are much lower than those of the solutions due to very thin films containing a fraction of PEG. However, it is quite consistent with the solution data shown in Fig. 2; by increasing the concentration of phthalocyanine in the base thin film of chlorophyllin, the chlorophyllin's peak at 404 nm begins to decrease significantly (Fig. 5a), while the peak at 630 nm is considerably broadened. Correspondingly, the visible range transmittance of the 1:3 hybrid remains at 85% (cyan

curve in Fig. 5b). A similar behavior is observed from the hybrid of chlorophyllin: Fe $_3O_4$ @Cu $_2$. $_x$ S. As shown in Fig. 5c, the 404 nm peak of chlorophyllin is significantly suppressed by increasing the concentration of Fe $_3O_4$ @Cu $_2$. $_x$ S. However, the 630 nm peak is only slightly modified at 1:3 (cyan curve in Fig. 5c). As can also be seen in Fig. 5c, there is a broad IR absorption between 700 nm 1400 nm for the hybrid 1:3 due to increasing amount of Fe $_3O_4$ @Cu $_2$. $_x$ S. Note that pure chlorophyllin and phthalocyanine have no NIR absorption. Accordingly, the visible transmittance is also maintained at 85% for hybrid 1:3 (cyan curve in Fig. 5d).

To investigate the effects of optical absorption on photothermal behaviors, the heating/cooling curves were experimentally obtained and presented in Fig. 6 for the thin films of chlorophyllin:phthalocyanine and chlorophyllin:Fe $_3O_4$ @Cu $_2$.xS hybrids. Note that all films were adjusted via concentration and thickness to exhibit AVT of 85% under

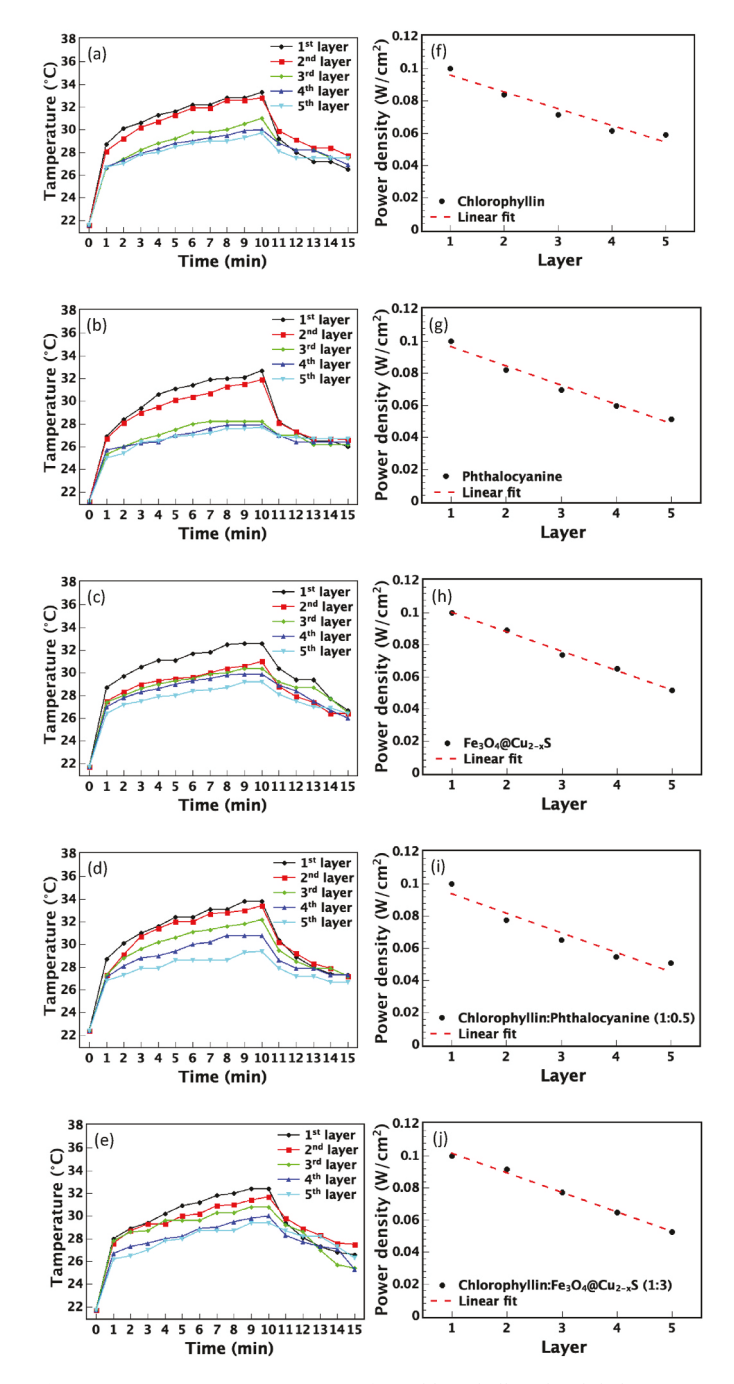


Fig. 7. Temperature vs. time curves of (a) chlorophyllin, (b) phthalocyanine, (c) chlorophyllin:phthalocyanine (1:0.5), (d) $Fe_3O_4@Cu_{2.x}S$, (e) chlorophyllin: $Fe_3O_4@Cu_{2.x}S$ (1:3) films under white-light irradiation in photothermal generator (PTG) with thermal insulation. Light power density vs. number of layers for the (f) chlorophyllin, (g) phthalocyanine(h) chlorophyllin:phthalocyanine (1:0.5), (i) $Fe_3O_4@Cu_{2.x}S$, and (j) chlorophyllin: $Fe_3O_4@Cu_{2.x}S$ (1:3) films. White light intensity is 0.1 W/cm². The room temperature is 22 °C.

white light irradiation. As shown in Fig. 6a, the temperatures of the chlorophyllin and phthalocyanine thin films respectively increase up to $13.39\,^{\circ}$ C and $12.53\,^{\circ}$ C from room temperature in 10 min under white light irradiation ($0.1\,$ W/cm²). Consistent with the absorptions of chlorophyllin and phthalocyanine (Fig. 5a), the UV absorption peak of the former is much greater than the latter, responsible for more efficient heating effect. The heating curves of all hybrids are between those of pure chlorophyllin and phthalocyanine (Fig. 6a). It is also consistent with the absorptions (Fig. 5a and c) that the chlorophyllin film (1:0,

black curve) and the $Fe_3O_4@Cu_{2.x}S$ film (0.1 purple curve) heat up to 13.39 °C and 15.34 °C, respectively (Fig. 6b) due to considerable IR absorption in $Fe_3O_4@Cu_{2.x}S$. As can also be seen in Fig. 6b, all other hybrids of chlorophyllin/ $Fe_3O_4@Cu_{2.x}S$ fall between the heating curves of pure chlorophyllin (1:0) and $Fe_3O_4@Cu_{2.x}S$ (0:1). Although chlorophyllin exhibits a strong UV peak at 404 nm, hardly any absorptions in the IR range. The broad IR absorption of $Fe_3O_4@Cu_{2.x}S$ is therefore responsible for the more pronounced heating effects.

As described above, since all films are transparent, light can then pass through multiple layers, generating heat on each one. Fig. 7 shows heating behaviors and light power density attenuation of the chlorphthalocyanine, chlorophyllin:phthalocyanine (1:0.5), onhyllin. Fe₃O₄@Cu_{2-X}S, and chlorophyllin:Fe₃O₄@Cu_{2-X}S (1:3) films in a photothermal generator (PTG) (Fig. 1). As shown in Fig. 7a-e, the temperatures of the top layers for chlorophyllin, phthalocyanine, chlorophyllin: phthalocyanine (1:0.5), Fe₃O₄@Cu_{2-X}S, and chlorophyllin:Fe₃O₄@Cu_{2-X}S $_{X}S$ (1:3) films can reach up to 33.3 °C, 32.7 °C, 32.6 °C, 33.8 °C, and 32.4 °C, respectively. Expectedly, the incident light experiences some attenuation as passing through multiple layers. Note that the light power density on the first (top) layer is a constant at 0.1 W/cm² for the PTG heating measurement. As shown in Fig. 7f-i, due to high transparencies of the films (85%AVT), the light power densities at the fifth layers in the cuboid can still reach power densities ranging from 0.05 to 0.06 W/cm². These film characteristics are particularly important in solar harvest and energy generation through multilayers in a three-dimensional (3D) fashion.

The molecular behaviors of the hybrids were studied with Raman spectroscopy. In this study, the excitation laser frequencies of Raman scattering were at 442 nm, 514 nm, and 633 nm. All samples were dropcasted on an aluminum foil. An earlier Raman study [24] on chlorophyllin and phthalocyanine showed close correlations between the absorptions and Raman peaks: the Raman peaks are significantly intensified if the excitation laser frequency is close to the absorption peak. As shown in Fig. 8a for chlorophyllin, the Raman peaks are identified as molecular vibrations involving bonds of the porphyrins, corresponding to the photon absorptions at UV and NIR. It is quite consistent with the absorption peaks at 404 nm and 603 nm for chlorophyllin that all Raman peaks are well enhanced by the excitations of 442 nm and 633 nm lasers while those are less intensified by the 514 nm laser due to low absorptions in the visible range (Fig. 8a). In a similar way, the Raman peaks of phthalocyanine are very sharp and strong as excited by the 442 nm and 633 nm laser since this porphyrin compound has a broad NIR absorption between 600 nm and 730 nm. One can also notice the UV absorption of phthalocyanine, responsible for considerable Raman peaks excited by 442 nm laser. There are virtually no Raman responses for the 514 nm laser for the same reason that phthalocyanine is quite transparent in the visible band.

As shown in Fig. 2c, Fe $_3O_4$ @Cu $_2$ - $_xS$ is characteristically exhibiting a wide IR absorption above 700 nm. Correspondingly, the sample excited by the 633 nm laser results in significant Raman peaks, and practically none is observed for the 514 nm laser. Only a small peak is visible for the 633 nm laser due to considerable UV absorption. The Raman peak at 474 cm $^{-1}$ is identified as the S $_2$ ions of CuS [38], while the one at 670 cm $^{-1}$ is associated with the Fe $_3O_4$ nanoparticles (Fig. 8c) [39].

Fig. 9 shows that the Raman spectra of chlorophyllin:phthalocyanine hybrids excited by the 442 nm laser. As shown in Fig. 9, the Raman peaks are consistently modified by the ratios of chlorophyllin:phthalocyanine from pure chlorophyllin (1:0) to pure phthalocyanine (0:1). At wavenumber 1525 cm⁻¹ [40], the Raman peak for 1:0 is consistent with that as shown in Fig. 8a for pure chlorophyllin (black curve) without any Raman peak from phthalocyanine. As more phthalocyanine is incorporated into the base chlorophyllin solution, a peak appears at 1525 cm⁻¹ for ratio 1:0.5 (red curve). Thereafter, the same peak intensifies at 1:1 (green), 1:2 (blue), 1:3 (cyan), and finally 0:1 (purple). This consistent Raman peak intensity enhancement indicates graduate increase of phthalocyanine fraction in the chlorophyllin base solution, that is

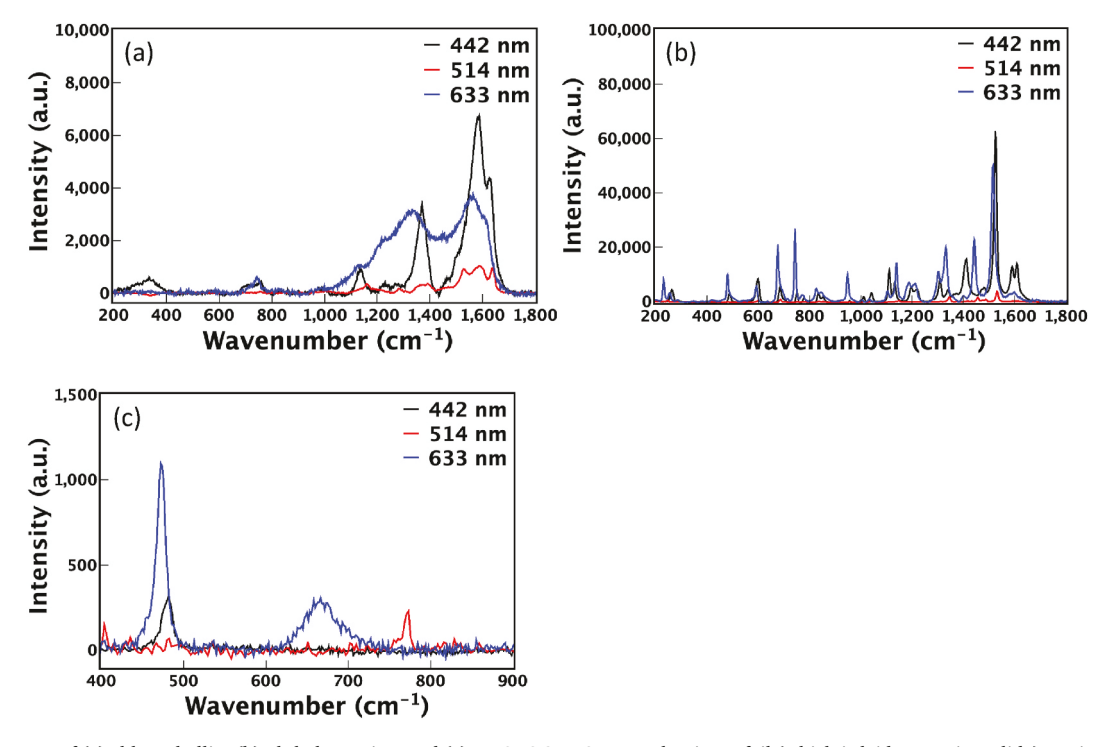


Fig. 8. Raman spectra of (a) chlorophyllin, (b) phthalocyanine, and (c) $Fe_3O_4@Cu_{2.x}S$ on an aluminum foil (which is laid on a micro slide), excited by 442 nm, 514 nm, and 633 nm lasers at room temperature.

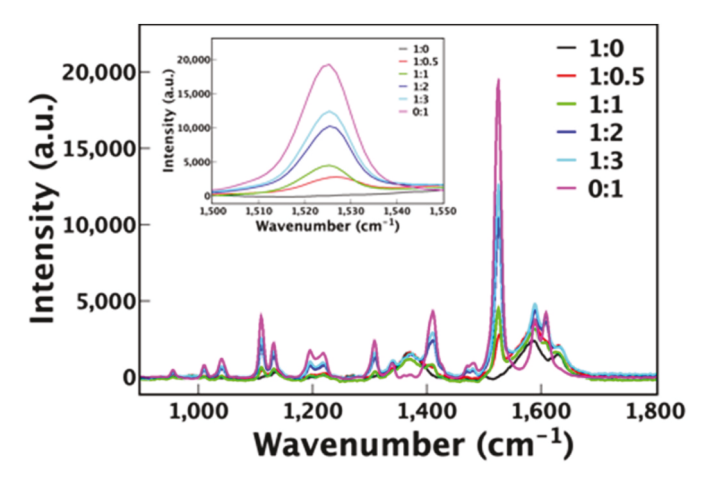


Fig. 9. Raman spectra of chlorophyllin:phthalocyanine hybrids of different ratios excited by $442~\mathrm{nm}$ lasers at room temperature.

responsible for the modified optical behaviors as shown in Fig. 2.

Consistent Raman spectra were also obtained for the hybrids of Chlorophyllin:Fe₃O₄@Cu_{2-x}S as shown in Fig. 10. As can be seen in Fig. 10 for excitation of 442 nm, the Raman spectrum of chlorophyllin (black) with increasing amount of Fe₃O₄@Cu_{2-x}S gradually involves from the base compound (1:0) to ratio 1:0.5 (red), 1:1 (green), 1:2 (blue), 1:3 (cyan), and finally pure Fe₃O₄@Cu_{2-x}S 0:1 (purple), which are consistent with those shown in Fig. 8a and c. The Raman spectra of the Chlorophyllin:Fe₃O₄@Cu_{2-x}S hybrids for the 1:0.5 ratio can be seen to exhibit Raman peaks assigned to both compounds: at 481 cm⁻¹ for Fe₃O₄@Cu_{2-x}S, and at 1373 cm⁻¹ and 1584 cm⁻¹ for chlorophyllin. By increasing the proportion of Fe₃O₄@Cu_{2-x}S, its Raman peak at 479 cm⁻¹ consistently increases from 1:0 (black) to 0:1 (purple). These Raman data indicate that the compositional variations in the hybrids can be continuously and congruently altered for spectral tuning purposes.

The thermal energy (Q) is defined as the heat generated by a

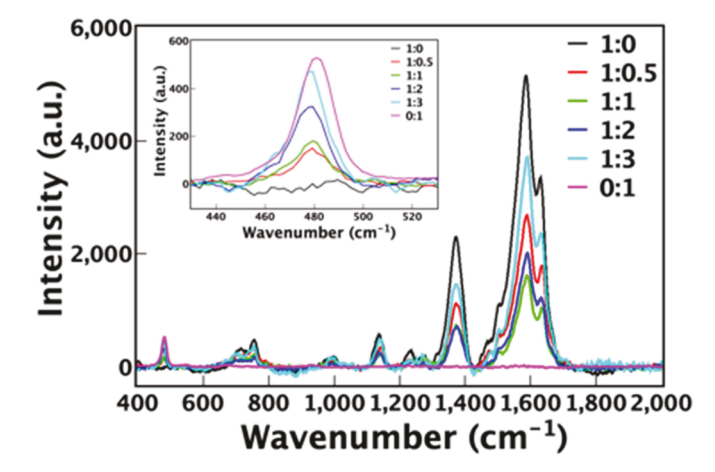


Fig. 10. Raman spectra of chlorophyllin: $Fe_3O_4@Cu_{2.x}S$ hybrids of different ratios excited by 442 nm lasers at room temperature.

photothermal thin film and it can be expressed as, where \dot{Q} is the input energy (solar simulator) and Δt is heating period [23,25]. In this research, the heating time is 10 min. Fig. 11 shows the thermal energy and power generated by each layer in the PTG. The calculated results are summarized in Table 1 and Table 2. As shown in these tables, the total thermal energy for chlorophyllin:phthalocyanine (1:0.5) and chlorophyllin: Fe₃O₄@Cu_{2-x}S (1:3) for five layers are, respectively, 3264.02 J and 3586.83 J; and the total power generated for chlorophyllin:phthalocyanine (1:0.5) and chlorophyllin: Fe₃O₄@Cu_{2-x}S (1:3) for five layers are, respectively, 5.44 W and 5.98 W. As a result of spectral tuning by compositional optimization, the hybrid materials can generate considerably greater total thermal energy and overall power than those by the pure compounds. The enhanced energy generation can be well correlated to the optical characteristics of the hybrids based on the intensified absorptions near UV and IR regions. Fig. 12 shows the energy density vs. number of layers for the hybrid films in the PTG. The calculated energy

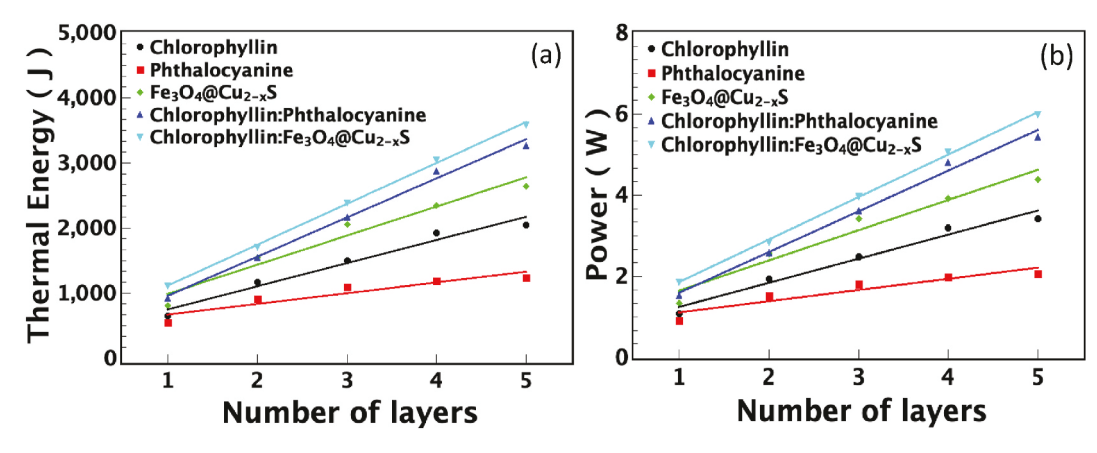


Fig. 11. (a) Thermal energy versus number of layers and (b) power versus number of layers in the cuboid as shown in Fig. 1.

Table 1Thermal energy (J) generated for different numbers of layers in the photothermal generator.

Number of layers	Chlorophyllin (J)	Phthalocyanine (J)	$Fe_3O_4@Cu_{2-x}S(J)$	Chlorophyllin:Phthalocyanine (1:0.5), (J)	Chlorophyllin: $Fe_3O_4@Cu_{2-x}S$ (1:3), (J)
1	646.15	547.99	804.91	920.10	1114.50
2	1166.89	913.75	1541.38	1548.97	1701.64
3	1494.99	1087.86	2052.59	2165.66	2380.78
4	1918.35	1186.29	2351.41	2877.70	3042.28
5	2049.33	1235.15	2636.65	3264.02	3586.83

Table 2Power (W) generated for different numbers of layers in the photothermal generator.

Number of layers	Chlorophyllin (W)	Phthalocyanine (W)	Fe ₃ O ₄ @Cu _{2-x} S (W)	Chlorophyllin:Phthalocyanine (1:0.5), (W)	Chlorophyllin:Fe ₃ O ₄ @Cu _{2-x} S (1:3), (W)
1	1.08	0.91	1.34	1.53	1.86
2	1.94	1.52	2.57	2.58	2.84
3	2.49	1.81	3.42	3.61	3.97
4	3.20	1.98	3.92	4.80	5.07
5	3.42	2.06	4.39	5.44	5.98

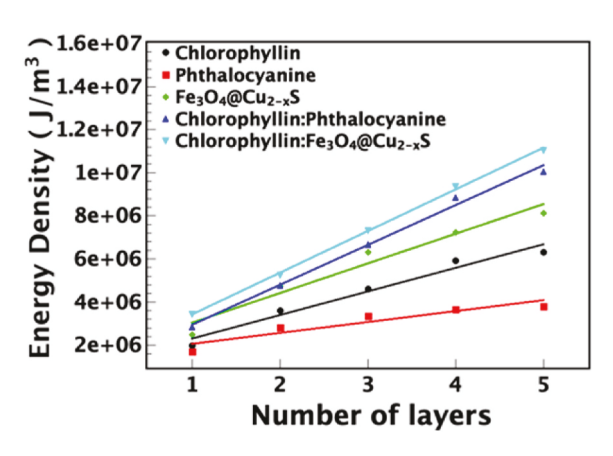


Fig. 12. Energy density versus number of layers in the cuboid as shown in Fig. 1.

density results are summarized in Table 3. As shown in Table 3, the total energy density for chlorophyllin:phthalocyanine (1:0.5) and chlorophyllin: Fe $_3$ O $_4$ @Cu $_2$ - $_x$ S (1:3) for five layers are 10043130.462 J/m³ and 11036398.154 J/m³, respectively, much greater than their single layer counterparts, showing amplified thermal energy by number of the transparent layers, which is the key novelty of 3D solar harvest.

4. Discussion

One of the key issues in this study deals with the structural and compositional effects on the photonic behaviors of porphyrin-based hybrids. For energy applications, spectral selectivity is crucial especially in solar harvesting via transparent thin films. For more efficient solar harvest, there is an increasing need to design and develop unique hybrids with the engineered properties. In this study, we identified both porphyrins and iron oxides for constructing unique porphyrin-based hybrids with spectral tunability. One of the challenges, however, lies on making congruent solutions between different material systems.

Table 3 Energy densities (J/m^3) for different numbers of layers in the photothermal generator.

Number of layers	Chlorophyllin (J/m³)	Phthalocyanine (J/m³)	$Fe_3O_4@Cu_{2\text{-x}}S~(J/m^3)$	Chlorophyllin:Phthalocyanine (1:0.5), (J/ $\rm m^3$)	Chlorophyllin: $Fe_3O_4@Cu_{2-x}S$ (1:3), (J/m ³)
1	1988163.692	1686112.615	2476656.000	2831084.308	3429216.000
2	3590418.462	2811544.615	4742717.538	4766056.615	5235823.385
3	4599969.231	3347257.846	6315662.769	6663577.846	7325484.923
4	5902615.385	3650123.077	7235113.846	8854465.846	9360869.538
5	6305621.538	3800470.154	8112771.692	10043130.462	11036398.154

Among the porphyrins, chlorophyllin is known to be a water-soluble compound, and only slightly soluble in chloroform and alcohol, while phthalocyanine can be partially dissolved in DMSO and THF. Fe $_3O_4@Cu_{2\cdot x}S$, as an oxide, is structurally and compositionally different from the porphyrins. The nanoparticles of Fe $_3O_4@Cu_{2\cdot x}S$ can be dispersed in toluene, chloroform, and THF. Since the water-soluble chemicals can be dissolved in THF, we developed a chlorophyllin aqueous solution in THF. In the same fashion, we were able to develop uniform solutions of phthalocyanine and Fe $_3O_4@Cu_{2\cdot x}S$ in THF. Based on these THF solutions, various hybrids were synthesized successfully with different ratios and congruently mixed with PEG for deposition of thin films via spin coating.

The photothermal effects of the porphyrins and iron oxides have been reported previously with different mechanisms [23]. The photothermal effects of metals and semiconductors are attributed to the so-called localized surface plasmon resonance (LSPR) [41-43]. A localized plasmon is the result of the confinement of a surface plasmon in a nanoparticle smaller than the wavelength of the incident light. A nanoparticle's response to the oscillating EM field can be described by the so-called dipole approximation of Mie theory [44]. The extinction cross-section of a particle depends on the dielectric function of the metal of which the particle is composed. This gives rise to very different absorption and scattering characteristics for different metal nanoparticles. At plasmonic resonance, the electric fields near the particle's surface are greatly enhanced, responsible for the photothermal effect. LSPR is mainly responsible for metals with large charge carriers. The porphyrin compounds are lacking of charge carriers, and their photothermal effects are identified to be associated with the molecular vibrations due to white light irradiation [23].

In Raman scattering, the laser light interacts with molecular vibrations of porphyrins, associated with phonons and electrons in the system, resulting in the energy shift of the laser photons. Stokes or anti-Stokes radiations are related to the vibrational energy levels in the ground electronic state of the molecule. Therefore, the Raman peaks shown in Figs. 9 and 10 are the direct measures of the molecular vibrational energies of in the hybrids. With three different lasers, 412 nm, 514 nm, and 633 nm, the Raman peaks are identified for both porphyrins [45] and Fe $_3$ O $_4$ @Cu $_2$ - $_x$ S [46]. The Raman peak of phthalocyanine between 1518 and 1530 cm⁻¹ corresponds to the main macrocycle stretching vibration [47]. The effects of hybrid on Raman peaks are clearly evident in Fig. 8. It can be seen in Fig. 9, the Raman peaks of chlorophyllin:phthalocyanine hybrids are shifted from 1518 cm⁻¹ (pure phthalocyanine) to 1526 cm⁻¹ (Fig. 9c), due to the interaction between phthalocyanine at 1518 cm⁻¹ and chlorophyllin at 1565 cm⁻¹. By changing the ratio of components, the Raman peak intensities experience graduate changes as shown in Figs. 9 and 10, indicating the continuous compositional evolution of the hybrid. In this fashion, the structures and compositions of the hybrids can be controlled for optimum optical properties in various energy applications. The experimental results show the significant increases in thermal energy and power generated by multiple transparent thin films in the PTG system (Fig. 11). As shown in Fig. 12, the energy density in the cuboid increases from $2831084.308 \text{ J/m}^3$ to $10043130.462 \text{ J/m}^3$ for chlorophyllin: phthalocyanine (1:0.5), a factor of 3.5; and from 3429216 J/m³ to $11036398.154 \text{ J/m}^3$ for chlorophyllin:Fe₃O₄@Cu_{2-X}S (1:3), a factor of 3.2 by increasing the number of layers from 1 to 5. These results indicate that both thermal energy and power can be further increase by adding more transparent layers.

A previous work utilized Fe3O4@Cu2-XS and chlorophyllin films for solar harvesting and photothermal energy generation [26]. However, both Fe3O4@Cu2-XS and chlorophyllin are synthetic compounds with given absorption characteristics. As shown in Fig. 2, the hybrids are spectrally tunable via compositional combinations. As a result of their structural flexibilities, the spectra of the hybrids can be compositionally altered for the optimum characteristics, i.e. even higher absorptions in the near UV and IR regions and further improved AVT. The optimized

optical and spectral characteristics will further enhance the efficiencies of solar harvesting and energy generation.

5. Conclusions

The novelty of this research lies on the design and synthesis of new porphyrin hybrids that exhibit not only strong absorptions preferentially in the near UV and IR regions, but also high average visible transmittance in the visible band. These unique photonic behaviors render the films optically transparent for photon collection through multiple layers in a 3D fashion. This new approach will profoundly transform solar harvesting from the conventional 2D to novel 3D structures for significantly increased solar harvesting surface area. Upon 3D solar harvesting, thermal energy is to be generated via a multilayer system that functions as an efficient solar light collector, energy converter and generator with much higher energy density. The experimental results of study demonstrate a concept of "Photo Thermal Generator" that can further convert heat to other forms of energy, such as electricity through thermoelectric.

In this study, we have designed and synthesized porphyrin-based hybrids, namely, chlorophyllin:phthalocyanine and chlorophyllin: Fe₃O₄@Cu_{2-x}S via controlled compositional combinations. The UV-Vis spectra of these hybrids are characterized and correlated to the components of chlorophyllin, phthalocyanine, Fe₃O₄@Cu_{2-x}S, and their hybrids. It is found that the optical spectra of the hybrids can be compositionally tuned by the ratios of the hybrid components resulting in well-enhanced absorptions in the UV and IR regions, while maintaining high AVTs for 3D solar harvest through multiple layers in a PTG. Using the solution method, uniform and transparent films of hybrids have been deposited on glass substrates for spectral selective solar harvest and photothermal energy generation. As the hybrid films are highly transparent, solar light is able to pass through multilayers and generate sufficient thermal energy in the photothermal generator. In this fashion, 3D solar harvest is achieved through multilayers with significantly increased energy density for both chlorophyllin:phthalocyanine (1:0.5) and chlorophyllin:Fe₃O₄@Cu_{2-X}S (1:3) hybrids. With only five transparent layers, the energy densities of both hybrids have increased by factor of 3.5 for chlorophyllin:phthalocyanine and 3.5 for chlorophyllin:Fe₃O₄@Cu_{2-X}S. Raman spectroscopy results show consistent structural evolutions in the hybrids with varied ratio of the components. By controlling the ratio of each component, the optical absorptions can be systematically tuned in both chlorophyllin:phthalocyanine and chlorophyllin:Fe₃O₄@Cu_{2-x}S for optimized solar harvest and photothermal energy generation.

Data availability statement

Data available in a publicly accessible repository.

CRediT authorship contribution statement

Jou Lin: Writing – original draft, Formal analysis, Data curation. Yuxin Wang: Formal analysis, Data curation. Mengyao Lyu: Formal analysis, Data curation. Zicheng Deng: Formal analysis, Data curation. Donglu Shi: Writing – review & editing, Writing – original draft, Visualization, Validation, Supervision, Resources, Project administration, Methodology, Investigation, Funding acquisition, Formal analysis, Conceptualization.

Declaration of competing interest

The authors declare that they have no known competing financial interests or personal relationships that could have appeared to influence the work reported in this paper.

Acknowledgement

We acknowledge the financial support from National Science Foundation CMMI-1635089 and CMMI-1953009.

References

- [1] G.W. Crabtree, N.S. Lewis, Solar energy conversion, Phys. Today 60 (3) (2007) 37-42
- [2] ASTM G173-03(2012), Standard Tables for Reference Solar Spectral Irradiances: Direct Normal and Hemispherical on 37° Tilted Surface, ASTM International, West Conshohocken, PA, 2012. Available from: http://www.astm.org/cgi-bin/resolver.cgi?G173.
- [3] B. Parida, S. Iniyan, R. Goic, A review of solar photovoltaic technologies, Renew. Sustain. Energy Rev. 15 (3) (2011) 1625–1636.
- [4] D. Poponi, Analysis of diffusion paths for photovoltaic technology based on experience curves, Sol. Energy 74 (4) (2003) 331–340.
- [5] M. Mehrtash, G. Quesada, Y. Dutil, D. Rousse, Performance Evaluation of Sun Tracking Photovoltaic Systems in Canada, 2012.
- [6] J.D. Mondol, Y.G. Yohanis, B. Norton, The impact of array inclination and orientation on the performance of a grid-connected photovoltaic system, Renew. Energy 32 (1) (2007) 118–140.
- [7] M.M. Fouad, L.A. Shihata, E.I. Morgan, An integrated review of factors influencing the perfomance of photovoltaic panels, Renew. Sustain. Energy Rev. 80 (2017) 1499–1511
- [8] M. Ito, K. Kato, H. Sugihara, T. Kichimi, J. Song, K. Kurokawa, A preliminary study on potential for very large-scale photovoltaic power generation (VLS-PV) system in the Gobi desert from economic and environmental viewpoints, Sol. Energy Mater. Sol. Cell. 75 (3–4) (2003) 507–517.
- [9] X. Zhou, J. Yang, F. Wang, B. Xiao, Economic analysis of power generation from floating solar chimney power plant, Renew. Sustain. Energy Rev. 13 (4) (2009) 736–749
- [10] T.M. Razykov, C.S. Ferekides, D. Morel, E. Stefanakos, H.S. Ullal, H.M. Upadhyaya, Solar photovoltaic electricity: current status and future prospects, Sol. Energy 85 (8) (2011) 1580–1608.
- [11] Technology Roadmap-Solar Photovoltaic Energy, International energy agency, 2010. http://www.iea-pvps.org.
- [12] The Solar Photovoltaic Electricity Empowering the World, EPIA report, 2011. http://www.greenpeace.org/international/en/publications/reports/Solar-Generation
- [13] A. Jäger-Waldau, M. Szabó, F. Monforti-Ferrario, H. Bloem, T. Huld, Lacal Arantegui R renewable energy snapshots. http://www.jrc.ec.europa.eu/, 2011.
- [14] M. Yamaguchi, H. Yamada, Y. Katsumata, K.H. Lee, K. Araki, N. Kojima, Efficiency potential and recent activities of high-efficiency solar cells, J. Mater. Res. 32 (18) (2017) 3445–3457.
- [15] K. Masuko, M. Shigematsu, T. Hashiguchi, D. Fujishima, M. Kai, N. Yoshimura, T. Yamaguchi, Y. Ichihashi, T. Mishima, N. Matsubara, S. Okamoto, Achievement of more than 25% conversion efficiency with crystalline silicon heterojunction solar cell, IEEE J. Photovoltaics 4 (6) (2014) 1433–1435.
- [16] J. Lin, Y. Zhao, D. Shi, Optical thermal insulation via the photothermal effects of Fe3O4 and Fe3O4@ Cu2- xS thin films for energy-efficient single-pane windows, MRS Commun. 10 (1) (2020) 155–163.
- [17] ARPA-E, Single-Pan Highly Insulating Efficient Lucid Designs (SHIELD) Program Overview, 2014.
- [18] D. Shi, M.E. Sadat, A.W. Dunn, D.B. Mast, Photo-fluorescent and magnetic properties of iron oxide nanoparticles for biomedical applications, Nanoscale 7 (18) (2015) 8209–8232.
- [19] M.E. Sadat, M. Kaveh Baghbador, A.W. Dunn, H.P. Wagner, R.C. Ewing, J. Zhang, H. Xu, G.M. Pauletti, D.B. Mast, D. Shi, Photoluminescence and photothermal effect of Fe3O4 nanoparticles for medical imaging and therapy, Appl. Phys. Lett. 105 (9) (2014), 091903.
- [20] M. Chu, Y. Shao, J. Peng, X. Dai, H. Li, Q. Wu, D. Shi, Near-infrared laser light mediated cancer therapy by photothermal effect of Fe3O4 magnetic nanoparticles, Biomaterials 34 (16) (2013) 4078–4088.
- [21] Z. Deng, J. Lin, S.L. Bud'ko, B. Webster, T.V. Kalin, V.V. Kalinichenko, D. Shi, Dual targeting with cell surface electrical charge and folic acid via superparamagnetic Fe3O4@ Cu2–xS for photothermal cancer cell killing, Cancers 13 (21) (2021) 5275.

- [22] Y. Zhao, M.E. Sadat, A. Dunn, H. Xu, C.H. Chen, W. Nakasuga, R.C. Ewing, D. Shi, Photothermal effect on Fe3O4 nanoparticles irradiated by white-light for energyefficient window applications, Sol. Energy Mater. Sol. Cell. 161 (2017) 247–254.
- [23] Y. Zhao, A.W. Dunn, D. Shi, Effective reduction of building heat loss without insulation materials via the photothermal effect of a chlorophyll thin film coated "Green Window", MRS Commun. 9 (2) (2019) 675–681.
- [24] Y. Zhao, J. Lin, D.M. Kundrat, M. Bonmarin, J. Krupczak Jr., S.V. Thomas, M. Lyu, D. Shi, Photonically-activated molecular excitations for thermal energy conversion in porphyrinic compounds, J. Phys. Chem. C 124 (2) (2019) 1575–1584.
- [25] M. Lyu, J. Lin, J. Krupczak, D. Shi, Light angle dependence of photothermal properties in oxide and porphyrin thin films for energy-efficient window applications, MRS Commun. 10 (3) (2020) 439–448.
- [26] M. Lyu, J. Lin, J. Krupczak, D. Shi, Solar harvesting through multilayer spectral selective iron oxide and porphyrin transparent thin films for photothermal energy generation, Adv. Sustain. Syst. (2021) 2100006.
- [27] M. Lyu, J. Lin, D. Shi, Solar desalination via multilayers of transparent photothermal Fe3O4@ Cu2-xS thin films, Energy Technol. 9 (11) (2021) 2100590.
- [28] Z. Lv, S. He, Y. Wang, X. Zhu, Noble metal nanomaterials for NIR-triggered photothermal therapy in cancer, Adv. Healthc. Mater. 10 (6) (2021) 2001806.
- [29] Q. Wang, H. Wang, Y. Yang, L. Jin, Y. Liu, Y. Wang, X. Yan, J. Xu, R. Gao, P. Lei, J. Zhu, H. Zhang, Plasmonic Pt superstructures with boosted near-infrared absorption and photothermal conversion efficiency in the second biowindow for cancer therapy, Adv. Mater. 31 (46) (2019) 1904836.
- [30] A. Tayyebi, O. Akhavan, B.K. Lee, M. Outokesh, Supercritical water in top-down formation of tunable-sized graphene quantum dots applicable in effective photothermal treatments of tissues, Carbon 130 (2018) 267–272.
- [31] V. Palmieri, M.D. Spirito, M. Papi, Graphene-based scaffolds for tissue engineering and photothermal therapy, Nanomedicine 15 (14) (2020) 1411–1417.
- [32] G. Liu, J. Xu, K. Wang, Solar water evaporation by black photothermal sheets, Nano Energy 41 (2017) 269–284.
- [33] M. Lyu, J. Lin, D. Shi, Solar Desalination via Multilayers of Transparent Photothermal Fe3O4@Cu2-xS Thin Films, Energy Technology, 2021, https://doi. org/10.1002/ente.202100590.
- [34] M. Wolf, J.I. Costa, M.B. Minameyer, T. Drewello, A.C. Tomé, D.M. Guldi, Efficient low driving force charge separation in an electron deficient Zn-Porphyrin fullerene donor-acceptor conjugate, J. Phys. Chem. C 123 (46) (2019) 28093–28099.
- [35] J. Lu, S. Liu, M. Wang, Push-pull zinc porphyrins as light-harvesters for efficient dve-sensitized solar cells. Front. Chem. 6 (2018) 541.
- [36] J. Lin, D. Shi, Photothermal and photovoltaic properties of transparent thin films of porphyrin compounds for energy applications, Appl. Phys. Rev. 8 (1) (2021), 011302.
- [37] Q. Tian, J. Hu, Y. Zhu, R. Zou, Z. Chen, S. Yang, R. Li, Q. Su, Y. Han, X. Liu, Sub-10 nm Fe3O4@ Cu2–x S core–shell nanoparticles for dual-modal imaging and photothermal therapy, J. Am. Chem. Soc. 135 (23) (2013) 8571–8577.
- [38] S.H. Chaki, J.P. Tailor, M.P. Deshpande, Covellite CuS-Single crystal growth by chemical vapour transport (CVT) technique and characterization, Mater. Sci. Semicond. Process. 27 (2014) 577–585.
- [39] P.C. Panta, C.P. Bergmann, Raman spectroscopy of iron oxide of nanoparticles (Fe3O4), J. Mater. Sci. Eng. 5 (1000217) (2015) 1000217.
- [40] M. Aydin, Comparative study of the structural and vibroelectronic properties of porphyrin and its derivatives, Molecules 19 (12) (2014) 20988–21021.
- [41] X. Huang, P.K. Jain, I.H. El-Sayed, M.A. El-Sayed, Plasmonic photothermal therapy (PPTT) using gold nanoparticles, Laser Med. Sci. 23 (3) (2008) 217–228.
- [42] K. Yang, S. Zhang, G. Zhang, X. Sun, S.T. Lee, Z. Liu, Graphene in mice: ultrahigh in vivo tumor uptake and efficient photothermal therapy, Nano Lett. 10 (9) (2010) 3318–3323.
- [43] M. Chu, H. Li, Q. Wu, F. Wo, D. Shi, Pluronic-encapsulated natural chlorophyll nanocomposites for in vivo cancer imaging and photothermal/photodynamic therapies, Biomaterials 35 (29) (2014) 8357–8373.
- [44] D.W. Hahn, Light Scattering Theory, Department of Mechanical and Aerospace Engineering, University of Florida, 2009.
- [45] M. Lutz, Resonance Raman spectra of chlorophyll in solution, J. Raman Spectrosc. 2 (5) (1974) 497–516.
- [46] M.H. Beyki, M. Shirkhodaie, F. Shemirani, Polyol route synthesis of a Fe 3 O 4@ CuS nanohybrid for fast preconcentration of gold ions, Anal. Methods 8 (6) (2016) 1351–1358.
- [47] C. Defeyt, P. Vandenabeele, B. Gilbert, J. Van Pevenage, R. Cloots, D. Strivay, Contribution to the identification of α-, β-and ε-copper phthalocyanine blue pigments in modern artists' paints by X-ray powder diffraction, attenuated total reflectance micro-fourier transform infrared spectroscopy and micro-Raman spectroscopy, J. Raman Spectrosc. 43 (11) (2012) 1772–1780.